ADVANCED MATERIALS
www.advmat.de

Thermal Disorder-Induced Strain and Carrier Localization Activate Reverse Halide Segregation

Nursultan Mussakhanuly, Arman Mahboubi Soufiani, Stefano Bernardi, Jianing Gan, Saroj Kumar Bhattacharyya, Robert Lee Chin, Hanif Muhammad, Milos Dubajic, Angus Gentle, Weijian Chen, Meng Zhang, Michael P. Nielsen, Shujuan Huang, John Asbury,* Asaph Widmer-Cooper,* Jae Sung Yun,* and Xiaojing Hao**

The reversal of halide ions is studied under various conditions. However, the underlying mechanism of heat-induced reversal remains unclear. This work finds that dynamic disorder-induced localization of self-trapped polarons and thermal disorder-induced strain (TDIS) can be co-acting drivers of reverse segregation. Localization of polarons results in an order of magnitude decrease in excess carrier density (polaron population), causing a reduced impact of the light-induced strain (LIS – responsible for segregation) on the perovskite framework. Meanwhile, exposing the lattice to TDIS exceeding the LIS can eliminate the photoexcitation-induced strain gradient, as thermal fluctuations of the lattice can mask the LIS strain. Under continuous 0.1 W cm^{-2} illumination (upon segregation), the strain disorder is estimated to be 0.14%, while at 80 °C under dark conditions, the strain is 0.23%. However, in situ heating of the segregated film to 80 °C under continuous illumination (upon reversal) increases the total strain disorder to 0.25%, where TDIS is likely to have a dominant contribution. Therefore, the contribution of entropy to the system's free energy is likely to dominate, respectively. Various temperature-dependent in situ measurements and simulations further support the results. These findings highlight the importance of strain homogenization for designing stable perovskites under real-world operating conditions.

1. Introduction

Metal halide perovskite semiconductors with the chemical formula ABX_3 (A: monovalent cation, B: divalent metal, X: halides) are promising candidates for deployment in next-generation photovoltaic technologies, and in more general optoelectronic devices, owing to their outstanding optical and electronic properties and potentially low fabrication costs.[1-4] Their bandgap can be tuned across the visible and near-infrared light spectrum by mixing halides and cations.[3,5] However, wide-bandgap (>1.65 eV) iodide and bromide mixed perovskites are prone to halide ion segregation upon photo-excitation.[6-8] This, in turn, results in an inhomogeneous local distribution of chemical elements, hence bandgap, across the perovskite absorber with adverse device performance impact.[9-12]

Many studies have been dedicated to understanding the driving forces for segregation and thereby subsequently mitigating this phenomenon. Bischak et al. showed that the polaronic effect, the interaction

N. Mussakhanuly, R. L. Chin, H. Muhammad, A. Gentle, W. Chen, M. Zhang, M. P. Nielsen, J. S. Yun, X. Hao
Australian Centre for Advanced Photovoltaics
School of Photovoltaic and Renewable Energy Engineering
University of New South Wales (UNSW)
Sydney 2052, Australia
E-mail: j.yun@unsw.edu.au; xj.hao@unsw.edu.au

The ORCID identification number(s) for the author(s) of this article can be found under https://doi.org/10.1002/adma.202311458

DOI: 10.1002/adma.202311458

A. M. Soufiani
Helmholtz-Zentrum Berlin für Materialien und Energie GmbH
Division Solar Energy
12489 Berlin, Germany
E-mail: arman.mahboubi_soufiani@helmholtz-berlin.de

S. Bernardi, A. Widmer-Cooper
Australian Research Council Centre of Excellence in Exciton Science
School of Chemistry
University of Sydney
Sydney 2006, Australia
E-mail: asaph.widmer-cooper@sydney.edu.au

J. Gan, J. Asbury
Department of Chemistry
The Pennsylvania State University
University Park, PA 16802, USA
E-mail: jba11@psu.edu

between the injected charge carriers and the soft ionic lattice, generates strain (light-induced strain, LIS) responsible for the separation of halide ions.[13] In addition, the inclusion of the less polar cation Cs^+ into the perovskite lattice by chemical manipulation was demonstrated to induce compressive strain on the lattice, eliminating segregation.[13–15] Strain-induced segregation was further discussed by Zhao et al., where segregation was shown to originate from grain boundaries due to local strain at these sites.[16] As a result, strategies to reduce grain boundaries, such as "epitaxial" growth of the thin films on a suitable substrate or growing perovskite with larger grains, were demonstrated to increase the activation energy for the migration of halide ions.[16–19] It has been further proposed that segregation can be initiated via defects within the perovskite absorber or at interfaces.[20,21] Many chemical agents have been demonstrated to be effective in the passivation of defects, hence suppressing segregation (e.g., KI, KBr, $C_{24}H_{51}OP$, or alloying Cl atoms).[22–26]

Studies on wide bandgap, mixed-halide perovskites show that the demixing of halides can be reversed by several means. Hoke et al. observed the splitting of X-ray diffraction (XRD) and photoluminescence (PL) peaks upon illumination and the recovery of the corresponding peaks after storing the samples in the dark, suggesting entropic reversibility of the segregated phases.[6] Mao et al. achieved uniform deformation of the perovskite lattice through saturation of the exposed region with polarons under high illumination intensities (10 W cm^{-2}, continuous wave). This eliminated the strain gradient driving halide segregation under low light intensities, enabling the entropy of mixing to homogenize the halide distribution.[27] However, studies on the effect of high temperatures show rather contradictory results. Spectral PL measurements of an ex situ sample heated to 70 °C indicated clear segregation of halide ions, concluding that the reversal effect observed in ref. [27] at high illumination, intensities could not be due to illumination-induced heating. On the other hand, Elmelund et al. demonstrated accelerated recovery of segregated phases at elevated temperatures (both in the dark and under illumination) using transient absorption spectroscopy.[28] In this case, a heat-induced increase in halide ion mobility was suspected to be responsible for overcoming the thermal barrier for halide remixing. It is, however, worth noting that the compositions in these two studies were quite different.

Since phase segregation is dependent on ion migration dynamics, one might expect the segregation of ions to be facilitated by increasing temperature.[6,13,29] However, an increase in the tendency of the halide ions to remix was also demonstrated at elevated temperatures,[28–31] indicating that thermodynamics is also essential. Given this disparity, the optoelectronic and structural changes causing the reversal of segregated phases upon rising temperature remain unclear.

Here, we find that the heat-induced reversal of segregation could be due to dynamic disorder-induced localization of polarons and due to thermal disorder-induced strain (TDIS), where both drivers could coactively reduce the impact of LIS. The reversal of segregation constantly quenched PL signal, reduced charge-carrier lifetime, and reduced excess carrier density, ascribed to dynamic disorder-induced localization of polarons. Temperature-dependent transient mid-infrared spectroscopy (TRIR) confirms the localization of polarons at elevated temperatures but with a reduced population (possibly due to a reduction in excess carrier density). Therefore, the LIS gradient within the perovskite lattice (otherwise responsible for segregation) could decrease. Given that the crossover from enthalpic to entropic dominance occurred ≈60–80 °C for our particular mixed-halide perovskite, the lattice strain disorder increased to 0.25% upon in situ heating the sample to 80 °C under continuous illumination (0.1 W cm^{-2}). Meanwhile, strain disorder at 80 °C under dark conditions (0.23%) exceeded the value imposed by 1-Sun illumination intensity (0.14%). Therefore, upon greater excitation of phonons, the anharmonic perovskite lattice could undergo more TDIS that may have a dynamic, distributed character, while thermal fluctuations of the perovskite lattice could mask photoexcitation-induced strain. Therefore, LIS could become weaker due to a decrease in excess carrier density. For the clarity of the novel insights, the outcomes from previous reports compared to this work are listed in Table S1 (Supporting Information). Extensive temperature-dependent in-situ measurements and theoretical simulations further support these findings. This enhanced understanding of the underlying driving forces responsible for segregation and thermally activated reversal could provide a pathway for designing stable and efficient wide-bandgap perovskites under real-world operating conditions.

2. Results and Discussion

2.1. PL Study of Heat-Induced Reversal of Halide Ions Segregation

We first monitor the time evolution of the PL spectrum while modulating the temperature to examine its impact on phase segregation. Throughout this study, triple-cation mixed-halide perovskite polycrystalline thin films (see Experimental Methods)

S. K. Bhattacharyya
Solid State and Elemental Analysis Unit (SSEAU)
Mark Wainwright Analytical Centre
UNSW Sydney, Sydney, NSW 2052, Australia
M. Dubajic
Department of Chemical Engineering and Biotechnology
University of Cambridge
Philippa Fawcett Drive, Cambridge CB3 0AS, UK
A. Gentle
School of Mathematical and Physical Sciences
University of Technology Sydney
Sydney 2007, Australia
M. Zhang
School of New Energy and Materials
Southwest Petroleum University
Chengdu 610500, China
S. Huang
School of Engineering
Macquarie University
Sydney 2109, Australia
A. Widmer-Cooper
The University of Sydney Nano Institute
The University of Sydney
Sydney, NSW 2052, Australia
J. S. Yun
Advanced Technology Institute
Department of Electrical and Electronic Engineering
University of Surrey
Guildford, Surrey GU2 7XH, UK

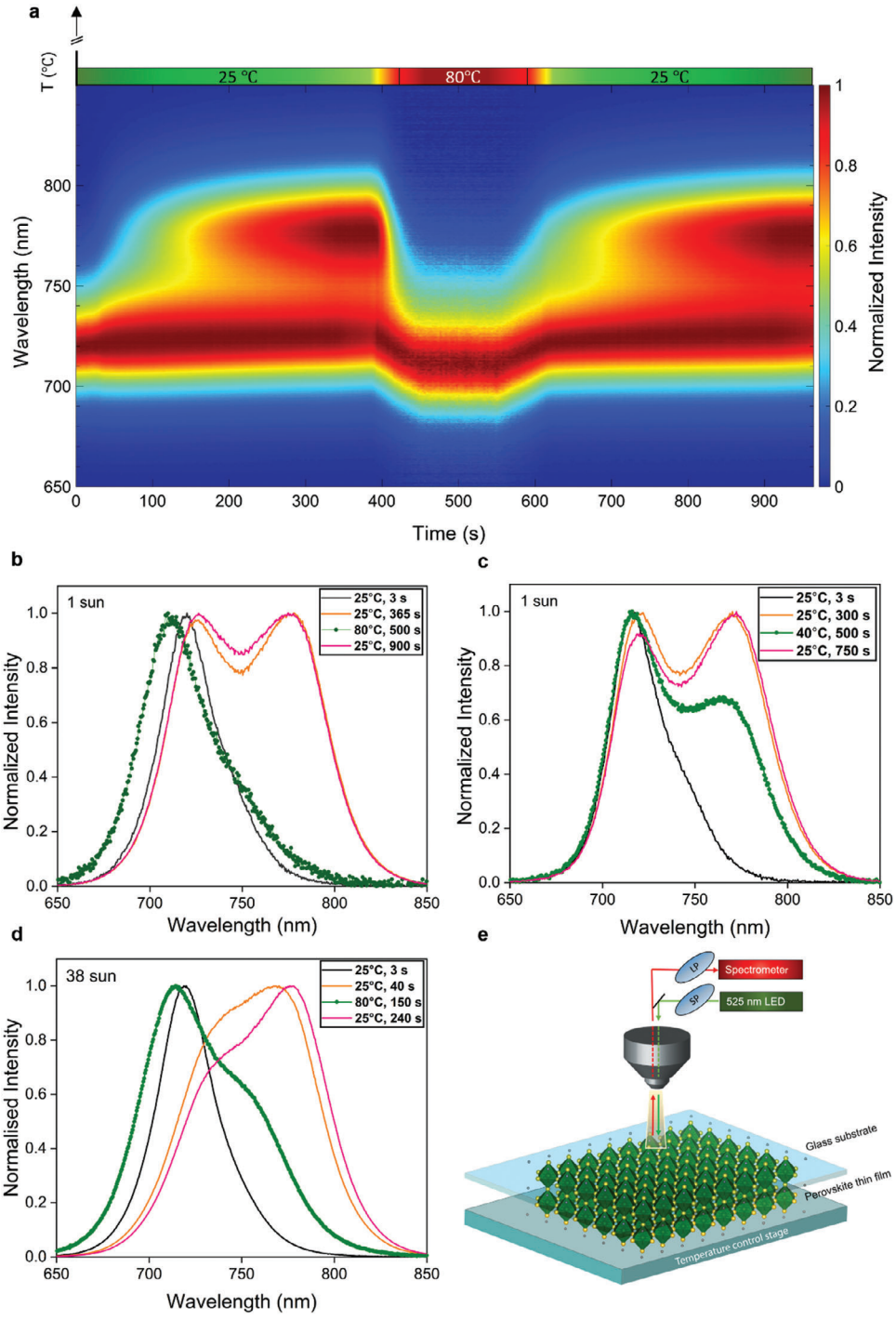

Figure 1. a) Normalized PL emission spectra map as a function of time for $Cs_{0.05}FA_{0.65}MA_{0.30}Pb\ (I_{0.70}Br_{0.30})_3$ perovskite, where sample temperature was raised to 80 °C and returned to room temperature, measured under 1-Sun equivalent illumination intensity. Selected normalized temperature-dependent PL spectra with the remixing temperature of b) 80 °C and c) 40 °C. d) Normalized temperature-dependent PL spectra were recorded under 38-Suns equivalent intensity using 80 °C as the in situ temperature of remixing. e) Schematic of the spectral PL measurement setup.

with the composition of $Cs_{0.05}FA_{0.65}MA_{0.30}Pb(I_{0.70}Br_{0.30})_3$ and thickness of ≈480 nm (mean grain size ≈380 nm) were used (Figure S1, Supporting Information). This composition is chosen because of its high susceptibility to segregation due to the large bromide fraction.[32] For all the spectral PL measurements conducted under ambient air conditions, the samples were mounted on a temperature-controlled cryo-stage, where the perovskite film directly contacts the stage to ensure proper heat transfer (**Figure 1e**). The illumination source is a light-emitting diode (LED) with a peak wavelength of 525 nm. An example

time-dependent spectral PL map with in situ controlled temperature is demonstrated in Figure 1a.

Upon photoexcitation at 1-Sun equivalent intensity, a peak emission associated with the pristine mixed-halide phase appears at ≈722 nm (≈1.71 eV), consistent with the absorption threshold of the as-deposited sample (Figure S2, Supporting Information). Over the first 300 s of continuous illumination, a new peak, commonly ascribed to the iodide-rich (I-rich) domain, appears at ≈772 nm, indicating the segregation of halide ions.[6,13] Immediately after increasing the temperature of the stage to 80 °C, the intensity of the PL peak at ≈772 nm attenuates, while a single emission peak associated with the initial mixed-phase, blue-shifted to ≈710 nm, is retained. Since the valence band maximum (VBM) in perovskite systems is formed by an antibonding combination between Pb *s* and X *p* orbitals, the alignment between X *p* orbitals and Pb-X bonds could be distorted at elevated temperatures, weakening the coupling.[33,34] Therefore, the VBM is likely to decrease in energy, resulting in the widening of the bandgap.[33–35] After cooling the sample back to room temperature, the main peak at ≈710 nm gradually redshifts to the phase segregation susceptible state (≈722 nm) with the gradual emergence of the I-rich phase at ≈772 nm. The above observations are seen in the selected PL spectra in Figure 1b. To isolate the impact of heat, a fresh perovskite sample was continuously illuminated until segregation features were clearly observed, and then the light source was turned off while the stage was heated to 80 °C for 2 min in the dark (Figure S3c, Supporting Information). The spectral PL map shows the disappearance of the low-energy peak at ≈772 nm after turning on the LED, possibly suggesting the disappearance of I-rich domains at high temperatures (here, 80 °C), thus a homogeneous distribution of halide species.[28] Interestingly, a clear PL signature of segregation does not appear upon turning on the light. Instead, the sample retains the high-temperature (80 °C) single PL peak signature at ≈710 nm. A similar response of segregation upon dark heating was observed at 60 and 40 °C. However, continuous heating at 40 °C could not sustain the mixed phase of halides after turning on the LED (Figure S3a, Supporting Information). The heat-induced reversal of segregation was further confirmed using fluorescence imaging microscopy with in situ temperature control (Figure S4, Supporting Information).

We then studied the response of segregation reversal to different temperatures, recording the temporal PL spectra under constant 1-Sun illumination (Figure S5, Supporting Information). The reversal of halide segregation could be already triggered at 40 °C (Figure 1c); However, the driving force is insufficient to entirely suppress the segregated I-rich phase. The decrease of the I-rich phase, rendering the spectral PL shape similar to that of the pristine film, was only observed at 60 °C and higher temperatures, with a corresponding shift of the mixed-phase emission peak to ≈713 nm at 60 °C (Figure S6b, Supporting Information).

The spectral PL signals were also recorded at illumination intensities higher than 1-Sun, with in situ heating. At high illumination intensities, the suppression of the I-rich peak (≈772 nm) becomes less prominent at elevated temperatures (Figure S8, Supporting Information). At 38-Sun equivalent illumination intensity, 80 °C could not entirely suppress the segregated phase PL signature (Figure 1d).

The change in the intensity of the high-energy PL peak associated with the mixed phase, as well as the intensity ratio of the low-energy peak (LE, 772 nm) to the high-energy peak (HE, 722 nm), are plotted in **Figures** 2a,b (Figures S7 and S9, Supporting Information) for different temperatures under 1-Sun illumination intensity. A correlation between the separation of halide ions and competitive charge-carrier recombination pathways can be seen. The segregation tends to occur during the increase and saturation of the PL intensity, indicative of the dominance of the radiative recombination rate; hence, an increase in excess carrier density (assuming the radiative recombination coefficient remains almost unchanged during the same period). However, the suppression of the I-rich PL peak upon increasing the temperature to 80 °C is accompanied by around a fifteen-times drop of the main PL peak intensity, indicative of increased non-radiative recombination rate (Figure 2a). Such PL quenching with increasing temperature could be due to the localization of polarons caused by thermal excitation of dynamic disorder (i.e., increased electron-phonon coupling rate).[36,37] Scattering of charge carriers with ionized impurities also could explain the decrease in PL intensity;[38] However, the scattering phenomenon with impurities is commonly understood to have a negligible impact on non-radiative charge-carrier recombination in halide perovskites.[38–40]

Relevant to the following discussion on the potential underlying mechanism of reversal of halide segregation, it is essential to note that in polar halide perovskites: (i) the coupling of excess electrons/holes with ionic lattice vibrations (phonons) form polarons;[41,42] (ii) polaron-induced strain gradient on perovskite lattice is proposed to be responsible for segregation;[13,27,43,44] and (iii) polaronic effect can be responsible for increasing non-radiative recombination rates (decrease in excess carrier density).[45,46] Upon illumination with 1-Sun light intensity, polarons are formed within the perovskite polycrystalline thin film due to their ionic nature.[40] Because of the charge funneling effect,[9] the mobile polarons/carriers diffuse toward the low bandgap regions, reported to be already existing in heterogeneous as-deposited films,[16,47] inducing strain gradient across the perovskite lattice, therefore promoting and stabilizing the segregated state of halide ions.[13]

Note that the steady-state PL discussed above is a directly related product of the excess carrier densities, which is influenced by both the generation rate and the charge-carrier effective lifetime. However, temperature-dependent ellipsometry revealed negligible variation in generation rate with increasing temperature (further discussed in Figure S10, Supporting Information). Therefore, the reduced excess carrier density and PL intensity at increased temperatures are mainly due to the increased non-radiative recombination rate but not the change in absorptivity.

To provide quantitative insight into the above PL results, the charge-carrier density and effective lifetime were analyzed at different temperatures by temperature-dependent, time and spectrally resolved PL measurements (2D TRPL). The samples were scanned in the 650–850 nm spectrum range, with a 7.5 nm step size, using a 532 nm pulsed laser (20 μJ cm^{-2}). The 2D TRPL maps at 25 and 40 °C reveal clear peaks at 722 and 772 nm, while at 80 °C the low energy peak, associated with the phase segregation, attenuates, consistent with the steady-state PL analysis (**Figure** 3a,b and Figure S11, Supporting Information). The

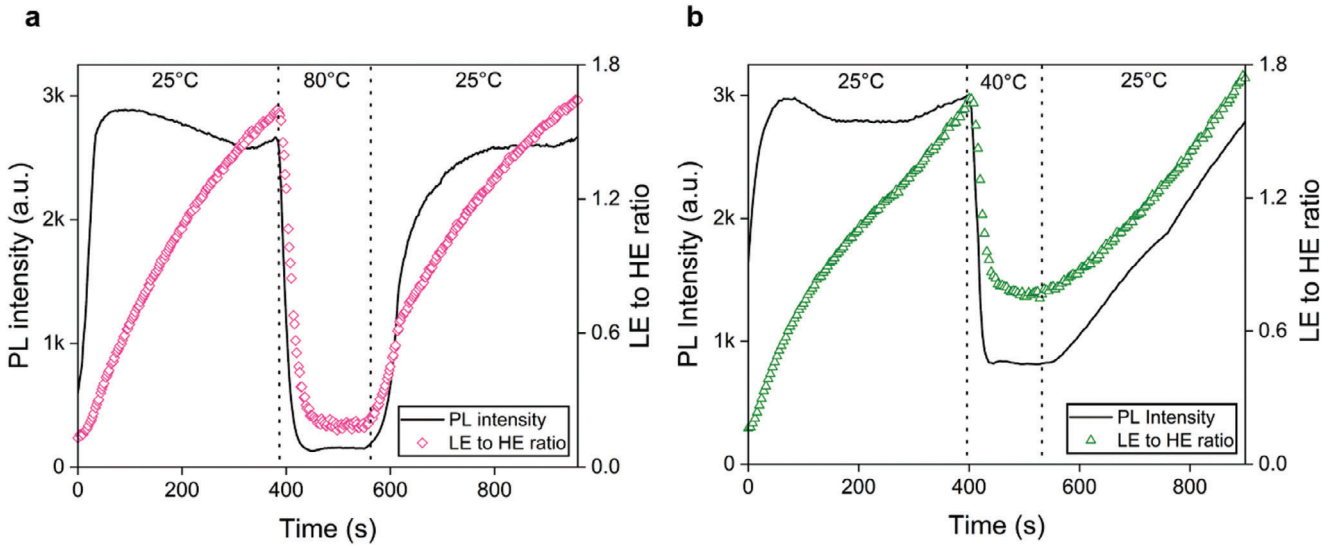

Figure 2. Change in the high-energy (HE) PL peak intensity and in the ratio of low-energy (LE) peak intensity to the HE peak intensity over time with respect to Figure 1b,c: a) sample heated to 80 °C under 1-Sun illumination intensity, b) sample heated to 40 °C under 1-Sun illumination intensity.

extracted effective carrier lifetime decreased from ≈950 ns at 25 °C to ≈800 ns at 40 °C and further to ≈330 ns as the temperature increased to 80 °C, consistent with the steady-state PL quenching (Figure 3c; Figure S12 and Table S2, Supporting Information). Meanwhile, the apparent carrier density reduced from $\approx 1.36 \times 10^{15}$ cm^{-3} (at 25 °C) to $\approx 1.19 \times 10^{15}$ cm^{-3} (at 40 °C) and further to $\approx 5.05 \times 10^{14}$ cm^{-3} (at 80 °C), respectively. We propose that dynamic disorder-induced localization of polarons is likely to activate non-radiative recombination pathways responsible for the decrease in excess carrier density.[36,37] Therefore, the strain gradient caused by excess carriers could decrease, which otherwise promotes segregation.[36,40,45] The non-radiative recombination rate upon heating, greater at higher temperatures, could indicate the formation of an increased number of localized polarons due to increased electron-phonon coupling rate, but not necessarily the increased total number of polarons in the whole illuminated region.

To check the corresponding changes in polaron dynamics with respect to the 2D TRPL, we further conducted temperature-dependent, time-resolved mid-infrared spectroscopy (TRIR). The samples were excited with a 532 nm pulsed laser (20 μJ cm^{-2}) with a 50 ns time delay and probed with continuous-wave IR radiation overlapped with the pulsed laser beam (see Experimental Section). A distinct absorption of large polarons appears between 800–1100 cm^{-1} (0.10–0.13 eV) that is higher at lower frequencies (Figure 3d). Interestingly, the absorption peak at ≈870 cm^{-1} shows a ≈30% decrease in amplitude (from ≈3450 μO.D. to ≈2400 μO.D.) as the temperature rose to 40 °C and further ≈50% (up to 1800 μO.D.) at 80 °C. This indicates a decreased polaron population due to decreased excess carrier density, evidenced by TRPL analysis (Figure 3c). Furthermore, the full width at half maximum of the mid-IR spectra shows an increasing trend (125.34 cm^{-1} at 25 °C, 138.08 cm^{-1} at 40 °C, 158.63 cm^{-1} at 80 °C) (Table S3, Supporting Information). The increasing breadth of FWHM results from the loss of the resonant enhancement of the absorption peak at the absorption onset of polaron absorption spectra (≈850 cm^{-1}) with rising temperature. According to Emin's large polaron model, such changes in absorption spectra indicate dynamic disorder-induced localization of polarons (further discussed in Figure S13a,b, Supporting Information).[36,48]

Further, the 2D frequency-time plot of respective TRIR spectra of large-polarons also reveals a widening of the absorption range from ≈930 cm^{-1} to ≈940 cm^{-1} at 40 °C and to ≈990 cm^{-1} at 80 °C despite the decreased intensity, which indicates more thermally activated phonon modes (Figure 3 e,f; Figure S14a-e and Table S4, Supporting Information). The excitation of more phonon modes is likely to increase electron-phonon coupling strength since (a) it leads to dynamic disorder in the perovskite lattice that increases the localization of polarons which promotes electron-phonon coupling;[36] (b) Excited phonons move the electronic states into nuclear configurations that are more anharmonic regions of their free energy surfaces. Both effects likely lead to increased non-radiative recombination rates and, thus, lower carrier density. Consequently, the system could exhibit a reduced population but more localized polarons, therefore, contributing to the reversal of segregation.

The interplay between the photo-excitation intensity (translated to excess carrier density) and temperature potentially dictates the strength of dynamic disorder and the electron-phonon scattering rate. The strength of dynamic disorder at temperatures up to 40 °C may not be sufficient to induce sufficient excitement of phonons to reduce excess carrier density. Therefore, a certain strain gradient would be present (see Figure 2b compared to Figure 2a). In other words, at temperatures below 40 °C, enthalpic contribution to the system's free energy still dominates; thus, the sample would be prone to segregation.

However, at higher temperatures, entropy is likely to take over the dominant role, contributing more to the free energy of the system, due to increased dynamic disorder causing greater localization of self-trapped polarons observed in the reduction of the resonant enhancement of polarons at their absorption onset from

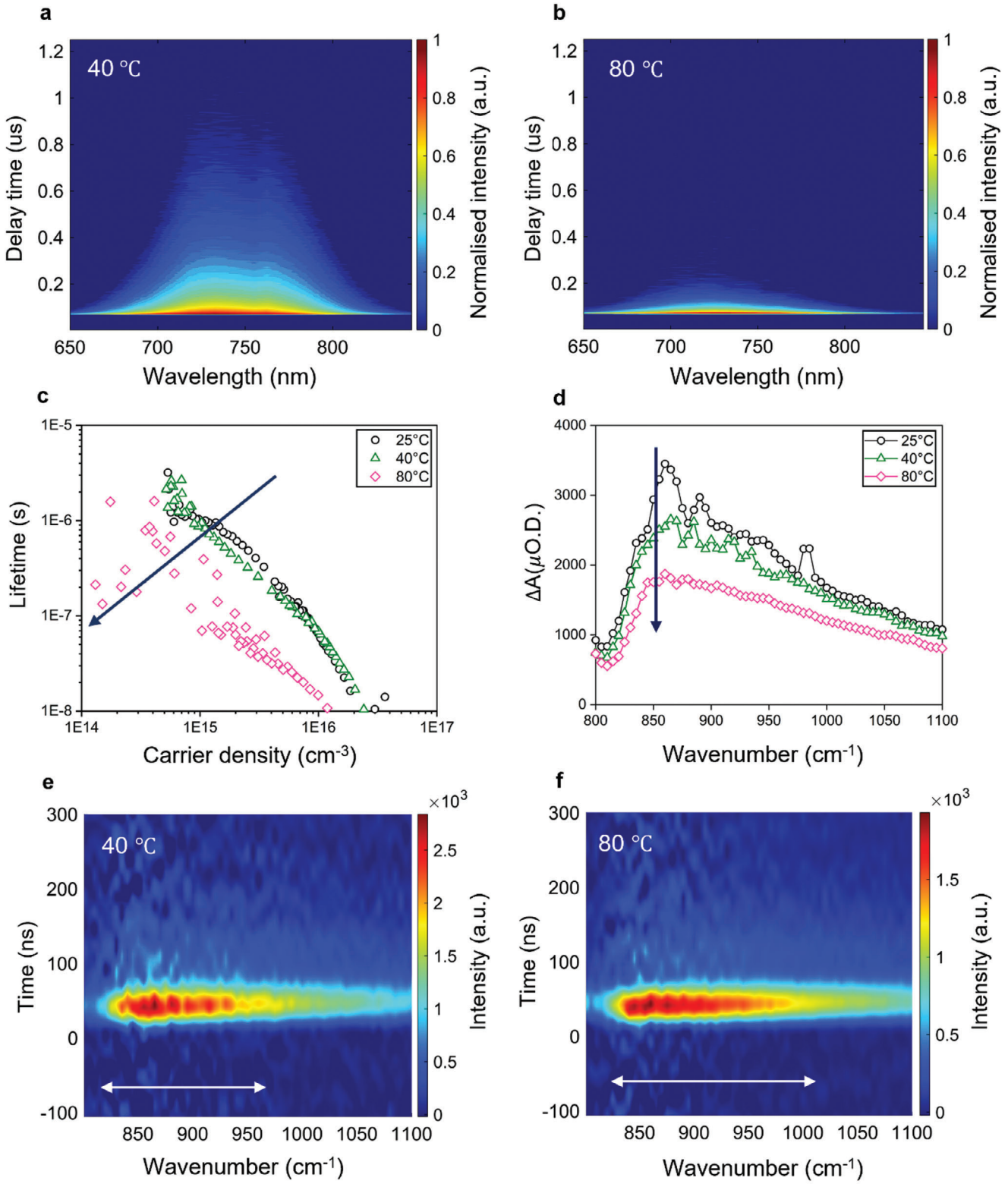

Figure 3. 2D TRPL results of samples measured at a) 40 °C b) 80 °C. c) Calculated charge carrier lifetime and excess carrier density from 2D TRPL (the blue line with an arrow represents excess carrier density under 1 Sun equivalent illumination intensity at the respective condition). d) Temperature-dependent, time-resolved mid-IR (TRIR) absorption spectra of $Cs_{0.05}FA_{0.65}MA_{0.30}Pb(I_{0.70}Br_{0.30})_3$ samples scanned at different temperatures 50 ns after bandgap excitation. The 2D frequency-time plot of the TRIR absorption spectra measured e) at 40 °C f) at 80 °C.

the TRIR measurements (Figure 3d; Figure S13a, Supporting Information). The data reveal that the crossover from enthalpic to entropic dominance occurs ≈60 – 80 °C for this mixed halide perovskite. Furthermore, if the enthalpic term is increased by injecting more excess carriers, the entropic term at 60 – 80 °C becomes too small to inhibit segregation. High levels of strain gradient could be maintained upon increasing the excess carrier density despite heating the sample to 80 °C. Therefore, more thermal energy is likely required to induce more dynamic disorder in the perovskite lattice (higher electron-phonon scattering rate) than under ≈1-Sun intensity at 80 °C; However, further temperature elevation to 100 °C and above for an extended period can decompose the perovskite framework.[49]

2.2. Insights from Simulation of Halide Ions Segregation and Remixing

To support the results discussed above, a recently developed model by Mao et al.[27] was used to study the segregation and remixing of halide ions under the influence of both light and temperature. This model includes the following effects: (1) Charge-carriers (polarons) attraction toward I-rich domains due to the charge funnelling; (2) A polaron-induced local strain gradient which attracts iodide ions; (3) Remixing of halide ions, for instance, due to vanishing local strain gradients. The model is based on the Kawasaki Hamiltonian, which is solved using a Monte Carlo (MC) method (for full details, see ref):[27]

$$H = -J \sum_{(i,j)^{2nd}} \sigma_i \sigma_j - \sum_i h_i \sigma_i \quad (1)$$

Here, the nodes (i, j) represent halide ions in the perovskite lattice and can locally exchange location only with neighbouring ions. J describes the interaction strength of the halide ions and determines the phase of the system (whether homogeneous or segregated) in the absence of light and at a temperature of 0 K. The coupling strength h_i represents the interaction between the halide ions and the photo-generated polarons (i.e., charge carriers).

The difference between h_i at adjacent sites represents the gradient in the strain that the polarons impose on the perovskite lattice and is the driving force for segregation. The polarons are modelled as Gaussian distributions with a standard deviation $\sigma \approx 3$ lattice sites. When considered in isolation, their effect is to locally alter the halide composition by favouring exchanges in which iodide ions can diffuse within the area delimited by the polaron. The LE domains act as traps for the charge carriers due to the charge funnelling effect, which causes carriers to diffuse toward these regions and preferentially recombine there.[50] The distribution of halide ions defines the local bandgap and biases the location of the polarons at each MC cycle.

This model was developed to rationalise the reversal of segregation under high illumination intensities and so does not include changes in the size of polarons as a function of temperature or the effects of crystallographic deformations; However, it does allow us to study competition between polaron-driven halide segregation and thermally driven reversal of segregation. For example, the driving force for segregation can disappear under very low illumination intensities (as the number of polarons falls below the threshold for segregation) or because of elevated temperatures, as the entropy of mixing due to heat wins over polaron strain. Because the lattice in the model cannot degrade, there always exists (for any given polaron strain) a temperature at which the entropic takeover takes place.

In this work, the halide composition of the lattice was set to 60% I and 40% Br. This is a high iodide concentration considering that fully segregated domains in $MAPb(Br_xI_{1-x})_3$ crystals reach I concentrations below 90%. This weakens the effect of polaron strain on the lattice compared to higher compositions in Br, thereby enhancing the relative magnitude of temperature-driven entropic mixing. The decision to use a ratio of (I/Br, 60:40) was based on practical considerations, as it proved challenging to capture the remixing behavior across a wide range of temperatures and illuminations with excessively high iodide concentrations.

Figure 4a (Figure S15, Supporting Information) displays the polaron distribution due to the interplay of temperature and illumination intensity (0.1 W cm^{-2}, 0.15 W cm^{-2} and 0.2 W cm^{-2}) after the model reaches a steady state condition. These illumination intensities are approximate values, and the equivalent polaron densities for the lattice model were calculated for a $MAPbBr_3$ single crystal (see ref. [27] for details). As the temperature in the model is expressed in units of the interaction strength J, it is not possible to directly relate it to a real sample temperature. Instead, the range of temperatures considered (0.5, 2, 5, and 10 in J units) as chosen based on the system's response. For example, ten corresponds to a temperature at which little segregation occurs (for any illumination intensity), i.e., at least 80 °C in the experiments, while 0.5 corresponds to room temperature behaviour.

The brighter regions in Figure 4a indicate a higher density of polarons. The shape and the size of the domains are defined by the local variation of the carrier density and the distribution of the halide ions. At room temperature and under 1-Sun illumination intensity, charge carriers funnel toward LE clusters due to chemical heterogeneity (or triggered by lattice imperfections), further promoting the segregation of halide ions.[13,47,51] Figure 4b (Figure S16, Supporting Information) shows the distribution of halide ions with respect to the formation of polarons in halide-segregated sites. Increasing the temperature at 1-Sun intensity, the halides partially remix and the islands of polarons become less defined. At this point, the contribution of entropy to the system's free energy is not yet sufficient to fully overcome the strain gradient, which is consistent with spectral PL results (Figure 1). If more charge carriers are now injected at constant temperature (0.15 W cm^{-2}), they funnel toward LE regions, increasing the strain gradient due to overlapped polarons around LE domains (yellow spots), leading to stronger HS. At sufficiently high temperatures (e.g., 80 °C), the entropic contribution to remixing is sufficiently high to overcome the strain gradient even at 0.15 W cm^{-2}.

This model shows that temperature-induced mixing is sufficient to explain the PL results; However, it does not include the physics relevant to describe global lattice deformations, temperature-induced reduction of carrier density (evident from TRPL), or increased carrier-lattice scattering

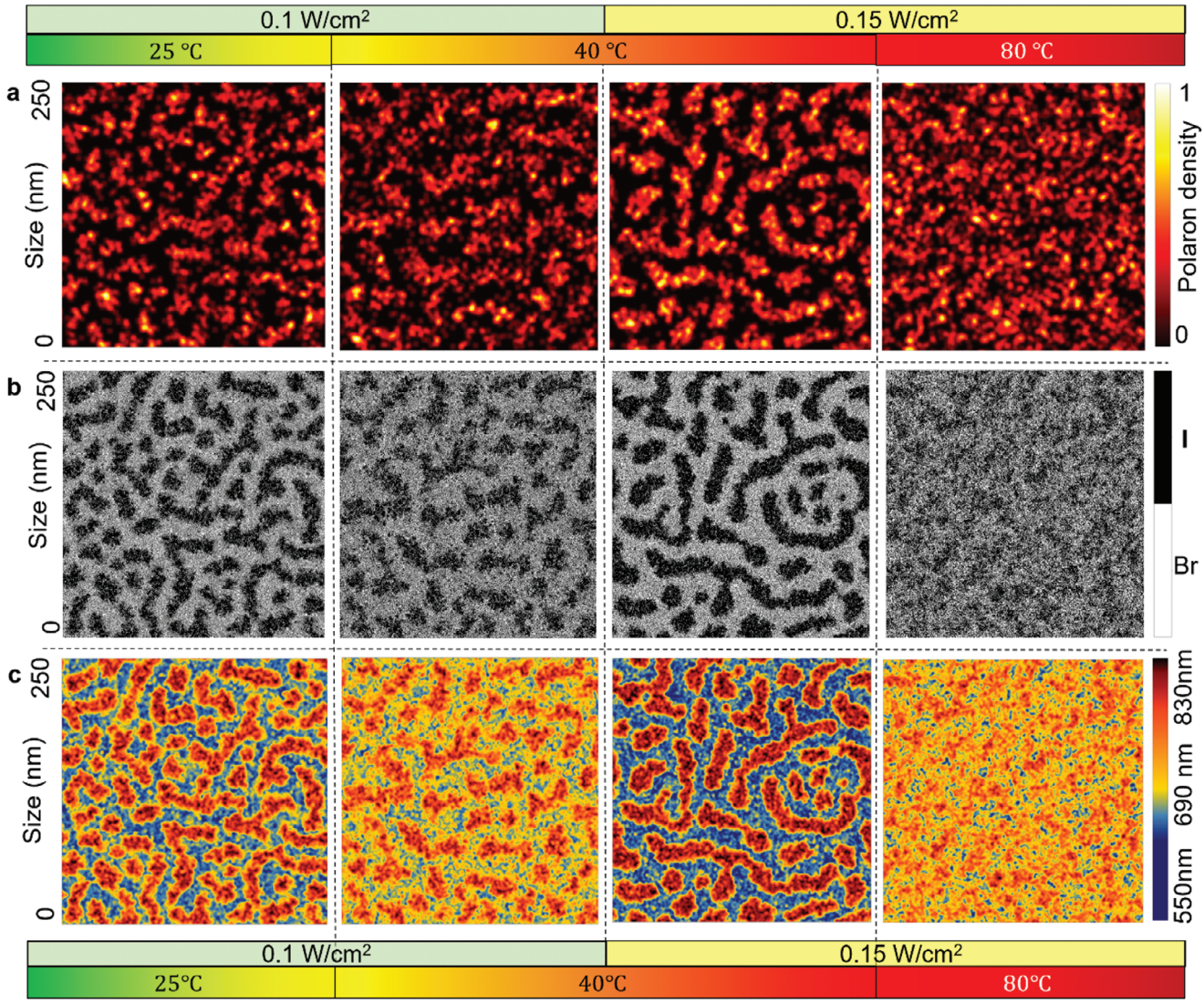

Figure 4. Simulation results showing halide ion segregation and reversal due to competition between light- and temperature-induced effects. The model considers: (1) the force attracting charge carriers toward LE domains; (2) the force that attracts I toward polarons due to the strain gradient; (3) the thermal driving force for homogenisation of halide ions. (a) Distribution of polarons at different temperatures and illumination intensities (0.1–0.15 W cm^{-2}). b) Distribution of halide species in response to the polaron distribution. c) Spacially resolved PL results.

(evidence from TRIR), and cannot, therefore, exclude a contribution from these effects. For example, the increased atomic vibrations at high temperatures could reduce polaron mobility due to localization (as evident from TRIR) and limit their capacity to funnel toward LE clusters, thereby causing the halide ions to remix and the bandgap across the material to become more uniform.

Figure 4c represents a simulated spatially resolved spectral PL map, where the red regions are associated with segregated LE I-rich emission domains (≈770 nm) corresponding to polaron islands in Figure 4a. The yellow emission corresponds to mixed regions (≈720 nm), and the orange to regions that are partially segregated. The complete simulation results for the temperature- and illumination-dependent polarons, halide ion distributions, and the spatial PL can be seen in Figures S15–S17 (Supporting Information).

2.3. Structural Examination of Halide Ions Segregation and Remixing

To experimentally evaluate structural changes contributing to segregation and reversal, we further conducted in situ temperature-dependent XRD measurements (see Figure S18, Supporting Information), both in the dark and under illumination at ≈0.1 W cm^{-2} intensity. Samples were scanned in the order of the following conditions (all in ambient air): (1) before illumination (RT, 25 °C); (2) under illumination; (3) under illumination with in situ heating; and (4) without illumination with in situ heat only. For conditions (2) to (4), the XRD scans were initiated three minutes after the illumination or heating modes (on/off) were changed. It is noted that illuminating the samples with ≈0.1 W cm^{-2} intensity using a white LED naturally increased the sample temperature to 35 °C.

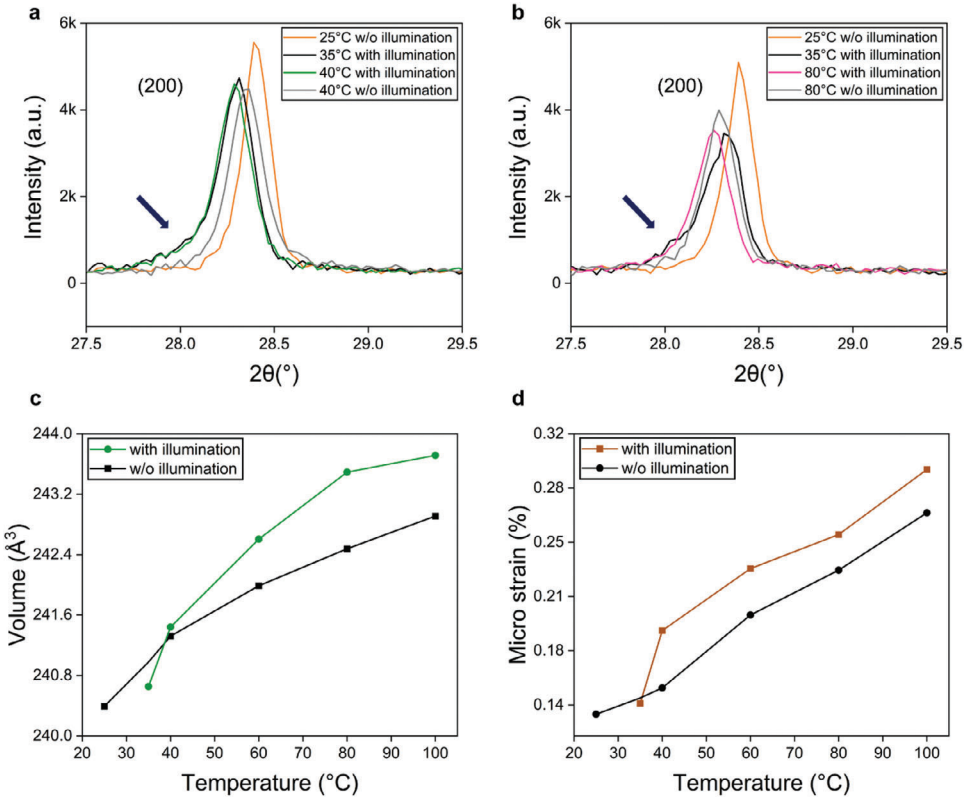

Figure 5. Temperature-dependent XRD pattern of (200) plane, measured on $Cs_{0.05}FA_{0.65}MA_{0.30}$ Pb $(I_{0.70}$ $Br_{0.30})_3$ perovskite thin-film in the following order: under dark, under illumination only (≈0.12 W cm^{-2}), under illumination with heating to a) 40 °C, b) 80 °C, and at an elevated temperature only without illumination, respectively (Figures S19 and S20, Supporting Information). c) Lattice parameters and d) extracted stain considering the full range XRD pattern (Figure S19, Supporting Information).

The XRD diffraction patterns of the pristine $Cs_{0.05}FA_{0.65}MA_{0.30}$ Pb $(I_{0.70}$ $Br_{0.30})_3$ sample revealed well-defined peaks representing the pm-3m cubic phase (Figure S19, Supporting Information). No apparent peaks associated with the non-photoactive phases were detected.[52] To facilitate the tracking of the changes in diffraction peak position and shape due to segregation, we focused just on the cubic phase 28.38° (200) peak.[6,53] Upon light soaking, all diffraction peaks decreased in intensity with a simultaneous peak broadening (Table S5, Supporting Information) and uniformly shifted to a lower 2θ angle compared with pristine mixed-halide phase (28.38° to 28.29°), implying loss of crystallinity, increased disorder, and light-induced expansion of the perovskite lattice, respectively (**Figures** 5a,b).[54,55] More importantly, a shoulder appears at 28.06°, indicating the segregation of the initial mixed phase into two crystalline phases (Figure 5a,b).

Since I-rich perovskites have a larger lattice constant than Br-rich perovskites, the emergence of the peak at a lower angle could correspond to the presence of I-rich domains.[6] Heating the sample to 80 °C during illumination attenuates the shoulder at 28.06°. Moreover, all diffraction peaks shifted to an even lower 2θ angle as the lattice expanded further with increased FWHM (from 28.29° to 28.21° for the (200) plane; see Figure 5b; Table S5, Supporting Information). Broadened diffraction peaks imply the presence of thermally activated structural disorder, consistent with TRIR results.[55,56] As the perovskite lattice thermally expands, the strain on the lattice tends to increase.[57,33] Therefore, unlike the reversal of segregation in the dark and at room temperature conditions due to entropy-driven relaxation of the lattice strain,[6] under illumination, entropy-driven reversal of segregation seems to be assisted with a vastly strained perovskite framework, confirmed by a shift of the individual diffraction peaks. In contrast, upon in situ heating to 40 °C, the shoulder corresponding to I-rich domains remains nearly unchanged (Figure 5a). In addition, the shift in the peak position is not significant (28.29° to 28.28°), indicating a minor change in the lattice constant and strain at moderate temperatures.

In the absence of illumination, in the 40 °C case, the selected diffraction peak slightly shifted to reside at 28.29°, between the pristine mixed-halide phase (28.38°) and illuminated-only (35 °C) conditions, implying a more substantial expansion of the lattice due to the presence of excess charge carriers (and photoexcitation-induced heating) at this moderate temperature (Figure 5a);[54] However, at 80 °C condition in the dark (i.e., absence of excess carriers), the expansion of the lattice is greater than under illumination with 1-Sun intensity. The peak is located at 28.26°, slightly lower than that at the illuminated-only condition (28.29°) (Figure 5b).[58] This is consistent with the notion that perovskite lattice can expand and hence get strained by heating, illumination, or under combined conditions.[54,58] Therefore, we propose to separate sources inducing strain: (1) strain on the lattice during the presence of excess carriers

(light-induced strain – LIS) and (2) strain imposed by heat – (TDIS). Since charge carriers funnel toward LE domains and generate strain gradients,[27] the LIS could have a more quasi-static character that leads to enthalpic pressure, causing segregation. However, upon greater excitation of phonons, the anharmonic perovskite lattice expands and could undergo more TDIS (reflected in the increased breadth of diffraction peaks) that may have a dynamic, distributed character. At elevated temperatures, the light-induced strain could become weaker (due to a decrease in excess carrier density and quasi-static nature), decreasing the enthalpic driving force of segregation, while TDIS could increase (due to dynamic, distributed nature), leading to the dominance of entropic term. Given that increasing strain on perovskite lattice could be responsible for the reduction carrier lifetime (translated into excess carrier density),[54] this proposed picture is consistent with the dominance of entropy of remixing upon reduced excess carrier density at elevated temperatures.

To quantify the response of the perovskite lattice to different conditions, the relative change of the lattice parameters and strain was obtained using a Pawley fit to the corresponding XRD diffraction peaks (see Experimental Section). At room temperature and in the absence of illumination, the volume of the pristine sample and the strain were calculated to be 240.39 $Å^3$ and ≈0.134% (see Figure 5c,d; Table S6, Supporting Information), implying the presence of minor strain on the lattice. Upon illumination, the lattice expanded to 240.65 $Å^3$, generating strain disorder equivalent to 0.141%. As the sample was heated to 40 °C, the lattice expanded further to 241.44 $Å^3$ with the increase of the strain disorder to 0.188%, while the most significant lattice expansion to 243.49 $Å^3$ was realized at 80 °C with a corresponding strain disorder of 0.250%. Therefore, the lattice exhibits higher expansion and greater strain disorder due to the combined effects of illumination and heating than the influence of each condition individually for a certain illumination intensity.

The changes in lattice properties due to only thermal disorder are consistent with the shifts of the diffraction peaks toward the lower angle (Figure S21b, Supporting Information). Interestingly, the TDIS at 40 °C (≈0.151%) is comparable to LIS generated under 1-Sun illumination intensity (≈0.141%); However, the TDIS value at 80 °C (0.227%) exceeds that imposed by the 1-Sun illumination (Figure 5d; Table S6, Supporting Information). We speculate that at 40 °C and 1-Sun illumination, with a lattice strain of 0.188%, LIS could contribute more to the total strain (0.188%) than TDIS, leading to dominant enthalpy. Therefore, halide ions reversal was less pronounced (see Figure 2b); However, upon illumination at 80 °C, the main contributor to the greater strain (0.250%) could be due to TDIS, spreading across the lattice and disrupting LIS gradients (as LIS decline due to a decrease in polaron density observed in 2D TRPL/TRIR analysis). Therefore, the enthalpic driving force of segregation could be counterbalanced. The perovskite framework is likely to be more ordered at low temperatures. So, the effect of LIS would be more significant because distortions influence their surroundings more strongly. In contrast, the strain induced by polarons could have a minor influence at higher temperatures because the disorder caused by thermal fluctuations could mask the changes in structure caused by LIS. We note that to fully isolate the impact of injected charge carriers, the effect of natural heating to 35 °C must be removed. Unfortunately, we could not run XRD scans under illumination with in situ cooling for this purpose due to the limitations of the custom-built setup. Moreover, due to the limited resolution of our XRD system, further in situ, nanoscale XRD investigations are needed.

3. Conclusion

This work provides novel insight into the causes driving the temperature-induced remixing of halide ions. We propose that the dominance of entropy of remixing at higher temperatures could be due to collegial drivers that potentially decrease the impact of the photo-induced strain. At first, dynamic disorder-induced self-trapping of polarons caused a one-order magnitude decrease in the excess carrier density; Therefore, the effect of the light-induced strain (LIS) could weaken. Meanwhile, immense global strain (here, TDIS) could eliminate the effect of local strain gradients as thermal fluctuations of the perovskite framework can mask the LIS due to its more dynamic, distributed nature. However, increasing the excess carrier density near the crossover temperature promotes the funneling of charge carriers toward low-energy sites, increasing the strain gradient and causing halide ions to segregate again. Therefore, the interplay between the enthalpy of segregation and entropy of remixing could be seen as an interplay between driving forces, LIS and TDIS. This enhanced understanding of the underlying driving forces responsible for segregation and thermally activated reversal could provide a pathway for designing optimally strained, stable and efficient mixed-halide, wide-bandgap perovskites under real-world operating conditions.

Supporting Information

Supporting Information is available from the Wiley Online Library or from the author.

Acknowledgements

X.H. acknowledges the financial support by Australian Research Council (ARC) Future Fellowship (FT190100756). J.S.Y. acknowledges the Royal Society research grant (RGS/R1/221369) and the support by the National Research Foundation of Korea (NRF) grant funded by the Korean government (MEST) (RS-2023-00257494 and 2022H1D3A2A01082324). J.G. and J.B.A. are grateful for support from the solar photochemistry program within the Division of Chemistry, Geosciences and Biosciences, Office of Basic Energy Sciences, Office of Science within the U.S. DOE through Grant DE-SC0019349. This work was financially supported by Australian Research Council (FT190100756), Australian Centre for Advanced Photovoltaics (ACAP), the Australian Research Council through the Centre of Excellence in Exciton Science (CE170100026), and by resources provided by the Pawsey Supercomputing Centre with funding from the Australian Government and the Government of Western Australia. M.P.N. thanks the UNSW Scientia Program for on-going support. N.M. would like to thank Alexander Baldacchino for the fruitful discussion. The authors acknowledge the use of the facilities at the Solid State and Elemental Analysis Unit, and the Australian microscopy and microanalysis research facilities at the Electron Microscope Unit, University of New South Wales (UNSW). Responsibility for the views, information or advice expressed herein is not accepted by the Australian Government.

Open access publishing facilitated by University of New South Wales, as part of the Wiley - University of New South Wales agreement via the Council of Australian University Librarians.

Conflict of Interest

The authors declare no conflict of interest.

Author Contributions

N.M. Conceived and designed experiments, fabricated samples, and conducted/assisted most of the characterizations and analysis. S.B. Developed and ran the simulation under supervision from A.W.C. J.G. performed and analyzed temperature-dependent TRIR measurement. S.K.B. Performed Pawley fitting of XRD data. R.L.C. and H.M. conducted and analyzed temperature-dependent 2D TRPL. A.G. conducted temperature-dependent ellipsometry. M.D. drew the schematics. W.C. performed temperature-dependent Fluorescence lifetime imaging. A.M.S., J.S.Y., and X.H. supervised the research. The manuscript was written by N.M. and revised by A.M.S., J.S.Y., X.H. through contributions from all authors.

Data Availability Statement

The data that support the findings of this study are available from the corresponding author upon reasonable request.

Keywords

carrier localization, halide segregation/reversal, mixed-halide wide-bandgap perovskite, strain, thermal/dynamic-disorder

Received: October 31, 2023
Published online: December 17, 2023

[1] M. A. Green, A. Ho-Baillie, H. J. Snaith, *Nat. Photonics* **2014**, *8*, 506.
[2] A. B. Djurisic, F. Z. Liu, H. W. Tam, M. K. Wong, A. Ng, C. Surya, W. Chen, Z. B. He, *Prog. Quantum Electron.* **2017**, *53*, 1.
[3] D. P. McMeekin, et al., *Science* **2016**, *351*, 151.
[4] S. De Wolf, J. Holovsky, S.-J. Moon, P. Löper, B. Niesen, M. Ledinsky, F.-J. Haug, J.-H. Yum, C. Ballif, *J. Phys. Chem. Lett.* **2014**, *5*, 1035.
[5] Z. Xiao, R. A. Kerner, L. Zhao, N. L. Tran, K. M. Lee, T.-W. Koh, G. D. Scholes, B. P. Rand, *Nat. Photonics* **2017**, *11*, 108.
[6] E. T. Hoke, D. J. Slotcavage, E. R. Dohner, A. R. Bowring, H. I. Karunadasa, M. D. Mcgehee, *Chem. Sci.* **2015**, *6*, 613.
[7] S. Draguta, O. Sharia, S. J. Yoon, M. C. Brennan, Y. V. Morozov, J. S. Manser, P. V. Kamat, W. F. Schneider, M. Kuno, *Nat. Commun.* **2017**, *8*, 200.
[8] D. J. Slotcavage, H. I. Karunadasa, M. D. Mcgehee, *ACS Energy Lett.* **2016**, *1*, 1199.
[9] M. Yuan, L. N. Quan, R. Comin, G. Walters, R. Sabatini, O. Voznyy, S. Hoogland, Y. Zhao, E. M. Beauregard, P. Kanjanaboos, Z. Lu, D. H. Kim, E. H. Sargent, *Nat. Nanotechnol.* **2016**, *11*, 872.
[10] T. Leijtens, K. A. Bush, R. Prasanna, M. D. Mcgehee, *Nat. Energy* **2018**, *3*, 828.
[11] A. J. Knight, J. B. Patel, H. J. Snaith, M. B. Johnston, L. M. Herz, *Adv. Energy Mater.* **2020**, *10*, 1903488.
[12] P. Gratia, G. Grancini, J.-N. Audinot, X. Jeanbourquin, E. Mosconi, I. Zimmermann, D. Dowsett, Y. Lee, M. Grätzel, F. De Angelis, K. Sivula, T. Wirtz, M. K. Nazeeruddin, *J. Am. Chem. Soc.* **2016**, *138*, 15821.
[13] C. G. Bischak, C. L. Hetherington, H. Wu, S. Aloni, D. F. Ogletree, D. T. Limmer, N. S. Ginsberg, *Nano Lett.* **2017**, *17*, 1028.
[14] L. A. Muscarella, et al., *ArXiv ACS Energy Lett.*, **2020**, *5*, pp. 3152–3158.
[15] E. M. Hutter, L. A. Muscarella, F. Wittmann, J. Versluis, L. Mcgovern, H. J. Bakker, Y.-W. Woo, Y.-K. Jung, A. Walsh, B. Ehrler, *Cell Rep. Phys. Sci.* **2020**, *1*, 100120.
[16] Y. Zhao, P. Miao, J. Elia, H. Hu, X. Wang, T. Heumueller, Y. Hou, G. J. Matt, A. Osvet, Y.-T. Chen, M. Tarragó, D. De Ligny, T. Przybilla, P. Denninger, J. Will, J. Zhang, X. Tang, N. Li, C. He, A. Pan, A. J. Meixner, E. Spiecker, D. Zhang, C. J. Brabec, *Nat. Commun.* **2020**, *11*, 6328.
[17] X. Tang, M. Van Den Berg, E. Gu, A. Horneber, G. J. Matt, A. Osvet, A. J. Meixner, D. Zhang, C. J. Brabec, *Nano Lett.* **2018**, *18*, 2172.
[18] A. F. Gualdrón-Reyes, S. J. Yoon, E. M. Barea, S. Agouram, V. Muñoz-Sanjosé, Á. M. Meléndez, M. E. Niño-Gómez, I. Mora-Seró, *ACS Energy Lett.* **2019**, *4*, 54.
[19] X. Wang, et al., *Nat. Commun.* **2019**, *10*, 1.
[20] A. Ruth, M. C. Brennan, S. Draguta, Y. V. Morozov, M. Zhukovskyi, B. Janko, P. Zapol, M. Kuno, *ACS Energy Lett.* **2018**, *3*, 2321.
[21] A. J. Knight, A. D. Wright, J. B. Patel, D. P. Mcmeekin, H. J. Snaith, M. B. Johnston, L. M. Herz, *ACS Energy Lett.* **2019**, *4*, 75.
[22] A. Al-Ashouri, *et al.*, *Science* **2020**, *370*, 1300.
[23] M. Abdi-Jalebi, Z. Andaji-Garmaroudi, S. Cacovich, C. Stavrakas, B. Philippe, J. M. Richter, M. Alsari, E. P. Booker, E. M. Hutter, A. J. Pearson, S. Lilliu, T. J. Savenije, H. Rensmo, G. Divitini, C. Ducati, R. H. Friend, S. D. Stranks, *Nature* **2018**, *555*, 497.
[24] J.-N. Yang, Y. Song, J.-S. Yao, K.-H. Wang, J.-J. Wang, B.-S. Zhu, M.-M. Yao, S. U. Rahman, Y.-F. Lan, F.-J. Fan, H.-B. Yao, *J. Am. Chem. Soc.* **2020**, *142*, 2956.
[25] R. A. Belisle, K. A. Bush, L. Bertoluzzi, A. Gold-Parker, M. F. Toney, M. D. Mcgehee, *ACS Energy Lett.* **2018**, *3*, 2694.
[26] J. Xu, et al., *Science* **2020**, *367*, 1097.
[27] W. Mao, C. R. Hall, S. Bernardi, Y.-B. Cheng, A. Widmer-Cooper, T. A. Smith, U. Bach, *Nat. Mater.* **2021**, *20*, 55.
[28] T. Elmelund, B. Seger, M. Kuno, P. V. Kamat, *ACS Energy Lett.* **2020**, *5*, 56.
[29] A. J. Knight, L. M. Herz, *Energy Environ. Sci.* **2020**, *13*, 2024.
[30] P. Nandi, C. Giri, D. Swain, U. Manju, S. D. Mahanti, D. Topwal, *ACS Appl. Energy Mater.* **2018**, *1*, 3807.
[31] A. D. Wright, J. B. Patel, M. B. Johnston, L. M. Herz, *Adv Mater* **2023**, *35*, 2210834.
[32] E. Aydin, T. G. Allen, M. De Bastiani, L. Xu, J. Ávila, M. Salvador, E. Van Kerschaver, S. De Wolf, *Nat. Energy* **2020**, *5*, 851.
[33] S. Meloni, G. Palermo, N. Ashari-Astani, M. Grätzel, U. Rothlisberger, *J. Mater. Chem. A* **2016**, *4*, 15997.
[34] W.-J. Yin, J.-H. Yang, J. Kang, Y. Yan, S.-H. Wei, *J. Mater. Chem. A* **2015**, *3*, 8926.
[35] H.-S. Kim, N.-G. Park, *NPG Asia Mater.* **2020**, *12*, 78.
[36] K. T. Munson, E. R. Kennehan, G. S. Doucette, J. B. Asbury, *Chem* **2018**, *4*, 2826.
[37] T.-R. Park, *Solid State Commun.* **1994**, *91*, 949.
[38] A. D. Wright, C. Verdi, R. L. Milot, G. E. Eperon, M. A. Pérez-Osorio, H. J. Snaith, F. Giustino, M. B. Johnston, L. M. Herz, *Nat. Commun.* **2016**, *7*, 11755.
[39] K. Wu, A. Bera, C. Ma, Y. Du, Y. Yang, L. Li, T. Wu, *Phys. Chem. Chem. Phys.* **2014**, *16*, 22476.
[40] D. W. Dequilettes, K. Frohna, D. Emin, T. Kirchartz, V. Bulovic, D. S. Ginger, S. D. Stranks, *Chem. Rev.* **2019**, *119*, 11007.
[41] A. M. Soufiani, F. Huang, P. Reece, R. Sheng, A. Ho-Baillie, M. A. Green, *Appl. Phys. Lett.* **2015**, *107*, 231902.
[42] C. Franchini, M. Reticcioli, M. Setvin, U. Diebold, *Nat. Rev. Mater.* **2021**, *6*, 560.
[43] D. T. Limmer, N. S. Ginsberg, *J. Chem. Phys.* **2020**, *152*, 230901.
[44] C. G. Bischak, A. B. Wong, E. Lin, D. T. Limmer, P. Yang, N. S. Ginsberg, *J. Phys. Chem. Lett.* **2018**, *9*, 3998.
[45] M. J. Schilcher, P. J. Robinson, D. J. Abramovitch, L. Z. Tan, A. M. Rappe, D. R. Reichman, D. A. Egger, *ACS Energy Lett.* **2021**, *6*, 2162.
[46] T. Kirchartz, T. Markvart, U. Rau, D. A. Egger, *J. Phys. Chem. Lett.* **2018**, *9*, 939.

[47] D. Kim, J. Lim, S. Lee, A. M. Soufiani, E. Choi, A. V. Ievlev, N. Borodinov, Y. Liu, O. S. Ovchinnikova, M. Ahmadi, S. Lim, P. Sharma, J. Seidel, J. H. Noh, J. S. Yun, *ACS Nano* **2021**, *15*, 20391.
[48] D. Emin, *Dev. Agric. Eng.* **1986**, *8*, 48.
[49] S. Kundu, T. L. Kelly, *EcoMat* **2020**, *2*, e12025.
[50] J. H. Noh, S. H. Im, J. H. Heo, T. N. Mandal, S. I. Seok, *Nano Lett.* **2013**, *13*, 1764.
[51] K. Frohna, et al., *Nat. Nanotechnol.* **2022**, *17*, 190.
[52] R. E. Beal, N. Z. Hagström, J. Barrier, A. Gold-Parker, R. Prasanna, K. A. Bush, D. Passarello, L. T. Schelhas, K. Brüning, C. J. Tassone, H.-G. Steinrück, M. D. Mcgehee, M. F. Toney, A. F. Nogueira, *Matter* **2020**, *2*, 207.
[53] A. J. Knight, J. Borchert, R. D. J. Oliver, J. B. Patel, P. G. Radaelli, H. J. Snaith, M. B. Johnston, L. M. Herz, *ACS Energy Lett.* **2021**, *6*, 799.
[54] H. Tsai, et al., *Science* **2018**, *360*, 67.
[55] H. Cho, S. Y. Back, J. H. Kim, O. Inturu, H. S. Lee, J.-S. Rhyee, *RSC Adv.* **2019**, *9*, 4190.
[56] S. Shahrokhi, M. Dubajic, Z.-Z. Dai, S. Bhattacharyya, R. A. Mole, K. C. Rule, M. Bhadbhade, R. Tian, N. Mussakhanuly, X. Guan, Y. Yin, M. P. Nielsen, L. Hu, C.-H. Lin, S. L. Y. Chang, D. Wang, I. V. Kabakova, G. Conibeer, S. Bremner, X.-G. Li, C. Cazorla, T. Wu, *Small* **2022**, *18*, 2200847.
[57] D. Liu, et al., *Nat Mater.* **2021**, *20*, 1337.
[58] N. Rolston, R. Bennett-Kennett, L. T. Schelhas, J. M. Luther, J. A. Christians, J. J. Berry, R. H. Dauskardt, *Science* **2020**, *368*, eaay8691.